

# PM<sub>2.5</sub> reduces the daytime/nighttime urban heat island intensity over mainland China



Zihao Feng <sup>a,b,c</sup>, Xuhong Wang <sup>a,b,c,\*</sup>, Mengqianxi Yu <sup>a,b,c</sup>, Yimei Yuan <sup>a,b,c</sup>, Bingqian Li <sup>a,b,c</sup>

<sup>a</sup> College of Urban and Environmental Sciences, Northwest University, Xi'an 710127, China

<sup>b</sup> Shaanxi Key Laboratory of Earth Surface System and Environmental Carrying Capacity, Northwest University, Xi'an 710127, China

<sup>c</sup> Shaanxi Xi'an Urban Forest Ecosystem Research Station, Northwest University, Xi'an 710127, China

## ARTICLE INFO

### Keywords:

Urban heat island  
Aerosol radiative forcing  
Particulate matter  
Sky conditions  
PM<sub>2.5</sub> level

## ABSTRACT

PM<sub>2.5</sub> pollution severely threatens people's living environment and health, significantly affect urban heat island (UHI). In this study, in-situ observed data were combined with satellite data via refined pollution intensity classification methods, and the relationships between PM<sub>2.5</sub> and canopy/surface UHI (CUHI/SUHI) were analyzed. PM<sub>2.5</sub> reduced the UHI in nearly all the environments, with more pronounced effects during clear-sky daytime and winter (-0.33 °C for the SUHI) and less pronounced effects at all-sky nights and in summer. For the former, PM<sub>2.5</sub> primarily diminishes the UHI intensity (UHII) by weakening incident radiation; this radiative forcing effect is exacerbated by the combination of PM<sub>2.5</sub> and high humidity, which is further amplified by winter pollution peaks. At night, the UHII primarily influenced by the initial temperature conditions during the day. Less intake of surface energy on high-pollution days, which in turn affects longwave radiation from the surface/canopy at night. Additionally, PM<sub>2.5</sub> has been found to significantly influence UHI through its interaction with potential influential factors and its filtering effect (different PM<sub>2.5</sub> levels correspond to varying conditions of these factors). This study with new insights into the impact of PM<sub>2.5</sub> on UHI could aid in the design of strategies to improve urban heat and pollution environments.

## 1. Introduction

Accelerated urbanization has transformed land use, changing the surface from natural to impervious, with an increase in high heat-retaining structures, such as buildings and roads, and a decrease in green spaces (Peng et al., 2011; Tran et al., 2006). Combined with significant anthropogenic heat emissions, this transformation has resulted in urban areas being warmer than their surrounding rural areas, a phenomenon known as the urban heat island (UHI) effect (Oke, 1973; Oke, 1984). On the other hand, the increase in the number of factories and vehicles, coupled with the increased consumption of fossil fuels and dense daily activities in urban areas, has exacerbated air quality issues, particularly particulate pollution (Jin et al., 2022; Yousefi et al., 2023). Fine particulate matter (PM<sub>2.5</sub>), with an aerodynamic diameter of 2.5 micrometers or less, can remain suspended in the air for extended periods. Long-term exposure to high concentrations of PM<sub>2.5</sub> increases the risk of respiratory and cardiovascular diseases (Sun et al., 2024; Zhou et al., 2015), whereas UHI exacerbate heat stress in urban residents

(Fahed et al., 2020; Gabriel and Endlicher, 2011). Understanding the relationship between PM<sub>2.5</sub> and UHI is not only an urgent academic need but also a crucial prerequisite for the sustainable development of urban environmental health.

Air pollution and UHI are closely related in urban environments. The higher temperatures in urban centers caused by UHI can accelerate photochemical reactions, leading to the accumulation of secondary pollutants and exacerbating air pollution (Wang et al., 2018). Additionally, different temperatures correspond to varying mixing rates of turbulence and boundary layer heights, further influencing PM<sub>2.5</sub> variations (Sarrat et al., 2006). The mechanisms by which PM<sub>2.5</sub> is affected by the urban thermal environment are relatively well understood. In contrast, the effects of fine particulate matter on UHI remain highly debated. During high-pollution events, PM<sub>2.5</sub> increases the optical thickness of aerosols, resulting in a stronger radiative forcing effect. During the day, the increase in fine particulate matter and haze aerosols enhances the reflection and scattering of shortwave radiation, reducing the heat received at the surface (Li et al., 2020; Ulpiani, 2021). Some

\* Corresponding author.

E-mail address: [jqy\\_wxh@nwu.edu.cn](mailto:jqy_wxh@nwu.edu.cn) (X. Wang).

scholars argue that aerosols absorb longwave radiation from the surface at night, further heating the air and increasing the UHII (Jacobson, 1998). For example, in their study of nighttime UHI and PM<sub>2.5</sub> in the Beijing–Tianjin–Hebei region during winter, Yuan et al. (Yang et al., 2020) reported that pollution enhances the minimum UHII (UHII<sub>min</sub>) through aerosol–cloud interactions. Cao et al. (Cao et al., 2016) reported that in semiarid cities, the average contribution of haze aerosols to the heat island effect is  $0.7 \pm 0.3$  K. However, the opposite viewpoint, that PM<sub>2.5</sub> has a cooling effect on nighttime UHI, is also widely noted. Yang et al. (Yang et al., 2021) suggested that high pollution effectively reduces the heat retention of the surface during the day, leading to decreased longwave radiation from urban canopy buildings at night and thus weakening the UHII. Through their study of the relationship between UHI and urban pollution island (UPI), Li et al. (Li et al., 2018) confirmed that UHI enhance the turbulent diffusion of particulates in urban areas, resulting in a negative correlation between the two.

In addition to affecting UHI through radiative forcing, PM<sub>2.5</sub> can also influence UHI by altering cloud properties (Wang et al., 2024), precipitation conditions (Zhao et al., 2024a), relative humidity (Guo et al., 2022), and convection intensity (Huang et al., 2018). Moreover, the factors influencing urban heat islands are highly complex. Wind can increase heat exchange between urban and rural areas (Li and Zhou, 2019), vegetation can rapidly reduce surface heat through evapotranspiration (Peng et al., 2018; Peng et al., 2011), and precipitation can promote the deposition of particulate matter and significantly lower ambient temperatures (Manoli et al., 2019). All these factors can contribute to reducing the UHI effect. In contrast, impervious surfaces and anthropogenic heat emissions are positively correlated with UHI (Ryu and Baik, 2012). Owing to the numerous factors influencing UHI, strict control of external conditions is essential for studying the mechanisms by which pollution affects the urban heat island effect. However, existing research often focuses on one or multiple cities and specific seasons (Cui et al., 2021; Yang et al., 2020), but for UHI, a three-month

period can result in significant differences in incoming radiative heat (Ali et al., 2024), potentially interfering with the research findings. Therefore, a study with a large sample size and strict control of conditions is necessary to accurately determine the impact of pollution on UHI and to clarify the applicability and precision of this mechanism.

To solve the existing problems in the current research, in situ and remote sensing observations of meteorological variables from 2015 to 2022 were collected, and a refined method for the classification and comparison of pollution was adopted to investigate the spatial correlation and heterogeneity between PM<sub>2.5</sub> and UHI at diurnal and nocturnal scales. Given the sensitivity of UHI to radiative balance, samples only within the same month were compared, and different sky conditions were distinguished to ensure similar background conditions across samples. This study enhances research standardization and universality while addressing gaps in understanding the mechanisms through which PM<sub>2.5</sub> impacts UHI, thereby providing scientific foundations for mitigating urban heat and particle pollution.

## 2. Materials and methods

### 2.1. Study area

As one of the countries with the widest latitudinal and longitudinal spans, China extends from approximately 73°33'E to 135°05'E longitude and 3°51'N to 53°33'N latitude. Mainland China encompasses diverse climatic zones with significant variations in aridity and humidity, alongside large variations in altitude (Fig. 1a). Serving as the habitat for 1.4 billion people, its urban and environmental conditions are severely impacted by the process of urbanization, particularly in densely populated eastern regions (Zhao et al., 2024b). In this research, 179 out of 333 secondary administrative regions were selected, and this screening method is provided in Text S3 of the supplementary file. The seasons are defined as winter (December–February), spring (March–May), summer

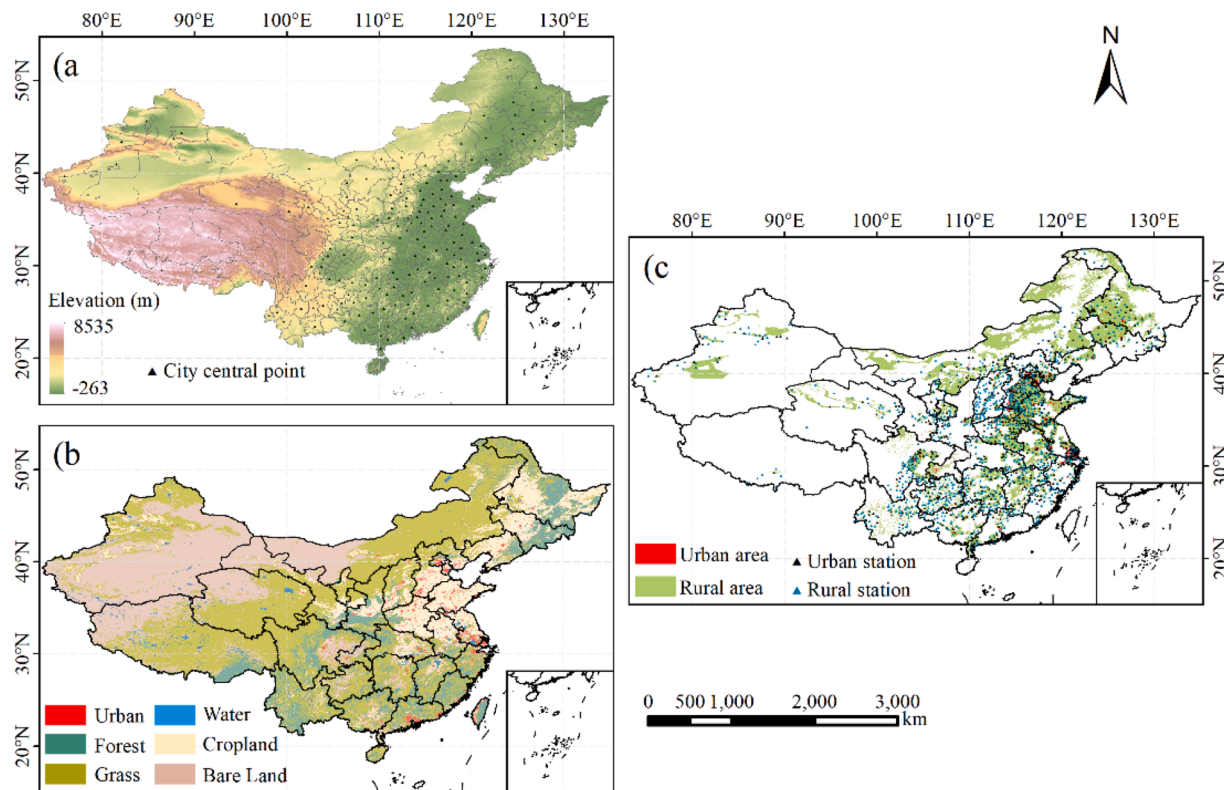


**Fig. 1.** Overview of the study area, (a) elevation and selected city locations, (b) land cover type (obtained from the MODIS Land Cover Type MCD12Q1 2022), (c) urban and rural stations and pixels (the details of urban–rural division and site selection are supplied in supplementary file Text S3).

(June–August), and autumn (September–November).

## 2.2. Data sources

Satellite data, in situ observation data, and reanalysis data were used to calculate the UHII and PM<sub>2.5</sub> levels, as well as to analyze the factors influencing UHI. The data sources are presented in Table 1, with detailed data descriptions given in the following sections.

### 2.2.1. Satellite data

Daily diurnal land surface temperature (LST) data from March 2015 to February 2023 were collected from the Aqua moderate resolution imaging spectroradiometer (MODIS) Land Surface Temperature and Emissivity global dataset (MYD11A1 V6.1) on the Google Earth Engine (GEE) (Wan et al., 2021), and the dataset was computed via the split window algorithm (McMillin, 1975). Daytime (LST\_Day\_1 km) and nighttime (LST\_Night\_1 km) LST data were used to calculate daytime/nighttime surface UHI (SUHI) (SUHI<sub>D</sub>/SUHI<sub>N</sub>), and their images were generated daily at 13:30 and 1:30, respectively. Strict quality control using the QC band was applied to eliminate pixels affected by clouds or with significant errors. No data imputation was performed; images in which the actual number of pixels divided by the maximum number of pixels was  $\leq 60\%$  were excluded from clear-sky day data analysis. Additionally, to ensure data availability under all-sky

**Table 1**

Details of the data acquisition process over mainland China from March 2015 to February 2023.

Data	Resolutions	Source
<b>Satellite data</b>		
<b>Land surface temperature (LST)</b> (Aqua MYD11A1 version 6.1) Daytime and nighttime LSTs	Spatial: 1 km Temporal: daily	NASA LP DAAC at the USGS EROS Center ( <a href="https://doi.org/10.5067/MODIS/MYD11A1.061">https://doi.org/10.5067/MODIS/MYD11A1.061</a> ) (Wan et al., 2021)
<b>Nighttime light (NTL)</b> VNP46A2	Spatial: 500m Temporal: daily	<a href="https://doi.org/10.5067/VIIRS/VNP46A2.001">https://doi.org/10.5067/VIIRS/VNP46A2.001</a>
<b>Land cover type</b> MCD12Q1	Spatial: 500 m Temporal: annual	NASA LP DAAC at the USGS EROS Center ( <a href="https://doi.org/10.5067/MODIS/MCD12Q1.061">https://doi.org/10.5067/MODIS/MCD12Q1.061</a> ) (Friedl and Sulla-Menashe, 2022)
<b>In-situ observation data</b>		
<b>Meteorological elements</b> maximum air temperature (T <sub>max</sub> ), minimum air temperature (T <sub>min</sub> ), precipitation (P), daytime/nighttime P(PD/PN), wind speed (WS), relative humidity (RH) sunshine duration (SD)	Temporal: daily	China Meteorological Data Service Center ( <a href="http://data.cma.cn/">http://data.cma.cn/</a> )
<b>Air pollution</b> PM <sub>2.5</sub> , daytime/nighttime PM <sub>2.5</sub> (PM <sub>2.5</sub> D/PM <sub>2.5</sub> N)	Temporal: hourly	China National Environmental Monitoring Centre ( <a href="http://www.cnemc.cn/">http://www.cnemc.cn/</a> )
<b>Reanalysis Data</b> <b>ERA5-Land Reanalysis</b> Solar radiation (SR), Albedo (Alb)	Spatial: 0.1° × 0.1° Temporal: daily	Copernicus Climate Change Service (C3S) Climate Data Store (CDS) (Muñoz Sabater, 2019)
<b>Auxiliary data</b> <b>Sky condition</b> Sky condition total coverage	Temporal: per 3 h	National Centers for Environmental Information ( <a href="https://www.ncei.noaa.gov/">https://www.ncei.noaa.gov/</a> )
<b>Digital elevation model (DEM)</b> (GTOPO30)	Spatial: 30 arc-seconds	U.S. Geological Survey (USGS) ( <a href="http://www.webgis.com/terr_world.html">http://www.webgis.com/terr_world.html</a> )

conditions, images where the actual number of pixels divided by the maximum number of pixels was  $\geq 30\%$  were retained for analysis.

Nighttime light (NTL) index data were obtained from the Visible Infrared Imaging Radiometer Suite (VIIRS) Lunar Gap-Filled Bidirectional Reflectance-Distribution Function (BRDF) Nighttime Lights dataset (VNP46A2) on the GEE. These data are produced by the Day–Night Band (DNB) of the VIIRS of the Suomi National Polar-orbiting Partnership (SNPP) (Román et al., 2018). This dataset underwent moonlight and atmosphere correction.

The land cover types from 2015 to 2022 were collected from the MODIS land cover type yearly global dataset (MCD12Q1 V6.1) of the GEE (Friedl and Sulla-Menashe, 2022). The LC\_Type1 used in this study was classified into 17 land use types on the basis of the International Geosphere-Biosphere Programme (IGBP) and was reclassified into 6 categories on the basis of the similarity between types (Fig. 1b).

### 2.2.2. In situ observation data

Daily meteorological element data were sourced from high-density surface station observations provided by the China Meteorological Data Service Center (<http://data.cma.cn/>), with more than 2,400 available stations nationwide. The data underwent rigorous quality control. Among them, maximum temperature (T<sub>max</sub>) and minimum temperature (T<sub>min</sub>) were used to calculate the daytime and nighttime canopy UHI (CUHI) (CUHI<sub>D</sub>/CUHI<sub>N</sub>), respectively.

Hourly PM<sub>2.5</sub> data were obtained from air quality monitoring stations provided by the China National Environmental Monitoring Centre (<https://www.cnemc.cn/>). Each day was defined as starting at 6:00 AM and ending at 6:00 AM the following day, with the daily average PM<sub>2.5</sub> concentration calculated from the '-24 h' value recorded at 6:00 AM on the second day. The PM<sub>2.5</sub> data from 6:00 AM to 6:00 PM were considered daytime PM<sub>2.5</sub>, whereas the data from 6:00 PM to 6:00 AM the next day were considered nighttime PM<sub>2.5</sub>. These values were calculated as the average of all included hourly data, excluding periods with fewer than 8 h of data.

### 2.2.3. Reanalysis data

In this study, the selected solar radiation (SR) data represent the total downward radiation received at the surface, obtained from the ERA5-Land dataset provided by the European Centre for Medium-Range Weather Forecasts (ECMWF). This dataset has a resolution of 0.1° × 0.1° and, along with albedo (Alb) data, is used for influencing factor analysis.

All raster data in this study were resampled to 1 km × 1 km via cubic convolution interpolation to achieve spatial-scale correspondence (Keys, 1981). The generation periods of nighttime LST (LST<sub>N</sub>) and T<sub>min</sub> are both between 1 and 4 am in the early morning, and in this study, they are considered nighttime heat island conditions of the previous day.

## 2.3. Methods

### 2.3.1. Urban/rural classification and UHII calculation

In this study, the simplified urban-extent (SUE) algorithm was applied to delineate urban and rural areas (Chakraborty and Lee, 2019). The specific steps were as follows.

- 1) The land cover types were reclassified into six basic categories, and the pixels exceeding ±50 m from the median of the built-up area of the city were removed in combination with the digital elevation model (DEM).
- 2) All built-up area pixels contained within the urban administrative boundaries are classified as urban areas, and other pixels (excluding water bodies, forests, ice and snow) are classified as rural areas.

Considering ongoing urbanization, this study defined urban areas using pixels classified as built-up areas in 2015 and rural areas using land cover types from 2022, excluding pixels where the land cover type

changed during this period. The urban–rural boundary derived by the SUE algorithm can be used to reduce the UHI anomalies caused by buffer size differences, and its reliability has been verified (Feng et al., 2023; Liu et al., 2022).

On the basis of this criterion, meteorological stations located where the number of urban pixels within a  $9 \times 9$  pixel window is  $\geq 5$  are classified as urban stations, whereas those located in rural pixels are classified as rural meteorological stations.

On the basis of the divided urban and rural areas and LST data, the SUHII can be determined as follows:

$$SUHII = \overline{LST_{Urban}} - \overline{LST_{Rural}} \quad (1)$$

Similarly, the CUHII can be calculated via the following formula:

$$CUHII = \overline{T_{Urban}} - \overline{T_{Rural}} \quad (2)$$

Where  $\overline{LST_{Urban}}$  and  $\overline{LST_{Rural}}$  are the mean urban and rural LSTs, respectively.  $\overline{T_{Urban}}$  and  $\overline{T_{Rural}}$  are the mean urban and rural temperatures, respectively, and the CUHII during the daytime and nighttime ( $CUHII_D$ / $CUHII_N$ ) is calculated with  $T_{max}$  and  $T_{min}$ , respectively.

### 2.3.2. Classification of clear/nonclear sky conditions on the basis of cloud cover calculations

Cloud cover refers to the fraction of the sky obscured by clouds. Conventional observation methods often rely on visual estimates made by observers, which can be subjective (Zhao et al., 2023). In addition, cloud volume data acquisition is difficult. The 3 h cloud volume data selected in this study cover only 400 sites in the country, which cannot meet the research needs. Therefore, on the basis of the strong correlation between cloud cover and sunshine duration (SD) (Aparicio et al., 2023), a threshold of sunshine hours corresponding to clear-sky conditions is set (Table 1). This approach helps reduce errors caused by human factors and improves data coverage.

The possible sunshine duration is defined as the maximum number of possible hours of sunshine at a given location and can be calculated via the following formula:

$$H_0 = \frac{2\cos^{-1}[-\tan\varphi\tan\delta]}{15} \quad (3)$$

$$\delta = 23.45\sin\left(360\frac{284+n}{365}\right) \quad (4)$$

where  $H_0$  is the possible sunshine duration,  $\varphi$  is the local latitude, and  $n$  is the day of the year starting on 1 January. Therefore, the percentage of sunshine duration (SD %) is defined as follows:

$$SD\% = \frac{SD_{Observed}}{H_0} \times 100\% \quad (5)$$

where  $SD_{Observed}$  is the actual SD at the meteorological station.

According to the total coverage code of the sky condition, clear-sky days are defined as follows: (1) cloud cover grades  $\leq 2$  (2/10–3/10, or few), (2) selected from 6:00 to 18:00 daily (including 5 data periods), with cloud cover grades  $\leq 2$  occurring more than 3 times and no periods with cloud cover grades  $> 5$ . After performing probabilistic statistics on the clear-sky SD % corresponding to all the selected stations, a 90 % cumulative frequency was used as the threshold, and the remaining 10 % of the sunshine percentage was discarded to increase the classification accuracy (Fig. 2). Therefore, a sunshine percentage exceeding 0.6 is considered indicative of clear-sky conditions.

### 2.3.3. Definition of high/low PM<sub>2.5</sub> levels for each month

The high/low pollution days of each city are divided according to the 25th and 75th percentiles of PM<sub>2.5</sub> in each month. The mean UHII of high-pollution days for the current month is subtracted from the mean UHII of low-pollution days for the same month, yielding the  $\Delta$ UHII for

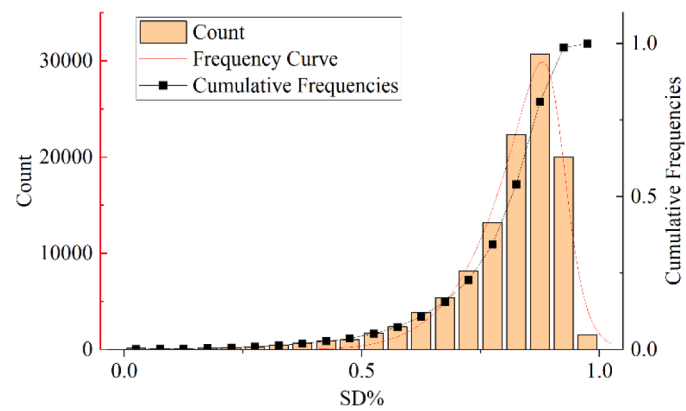


Fig. 2. The number of occurrences and cumulative frequency of different percentages of SD under clear-sky conditions (defined by the total coverage code of sky conditions).

the current month. This process is repeated for each month of the study period, and the final  $\Delta$ UHII for each city for the current month is obtained by averaging all the  $\Delta$ UHII values for the same month across the study period.

If the current year is  $m$  and the month is  $i$ , with Q<sub>25th</sub> and Q<sub>75th</sub> representing the 25th and 75th percentiles of PM<sub>2.5</sub> for the current month, the  $\Delta$ UHII for the city in month  $i$  of year  $m$  is calculated as follows:

$$\Delta UHII_{m,i} = \overline{UHII_{m,i}(Q_{75th})} - \overline{UHII_{m,i}(Q_{25th})} \quad (6)$$

where  $\overline{UHII_{m,i}(Q_{75th})}$  is the mean UHII for all days in month  $i$  of year  $m$ , with PM<sub>2.5</sub> levels above the 75th percentile and where  $\overline{UHII_{m,i}(Q_{25th})}$  is the mean UHII, with PM<sub>2.5</sub> levels below the 25th percentile. Therefore, the  $\Delta$ UHII for month  $i$  in the city is defined as follows:

$$\Delta UHII_i = \frac{\sum_{m=2015}^{2022} \Delta UHII_{m,i}}{n} \quad (7)$$

where  $n$  is the number of years within the study period, with  $n=8$  in this study (no invalid data condition). If in any given year, the number of high- or low-pollution days for a particular month is less than or equal to 2, that month is excluded from the analysis.

This study employed the random forest (RF) regression model (Breiman, 2001) and Spearman correlation analysis (Zar, 2005) to investigate influential factors and correlations. Both methods are excellent techniques for nonparametric analysis, and the RF model performs well in exploring both linear and nonlinear relationships (He et al., 2024; Liu et al., 2018).

## 3. Results

### 3.1. Distribution of pollution and UHI

#### 3.1.1. Annual and seasonal distributions of PM<sub>2.5</sub>

From 2015 to 2022, the regions with the lowest annual average pollution levels were concentrated in the southeastern and southwestern parts of mainland China. A trend was observed both during the day and at night (Fig. 3). Conversely, heavily polluted areas are concentrated at approximately 35°N, with the PM<sub>2.5,N</sub> concentration slightly higher than that during the day. The highest latitudinal profile averages are 55.6 (PM<sub>2.5,N</sub>) and 52.1  $\mu\text{g}/\text{m}^3$  (PM<sub>2.5,D</sub>), respectively. This is attributed to the higher proportion of industry (Jin et al., 2022) and greater traffic pressure (Ping et al., 2023) in this region, leading to more severe emissions of pollutants, such as dust, than in other areas. Additionally, the northwestern part of China, located in the temperate desert region,

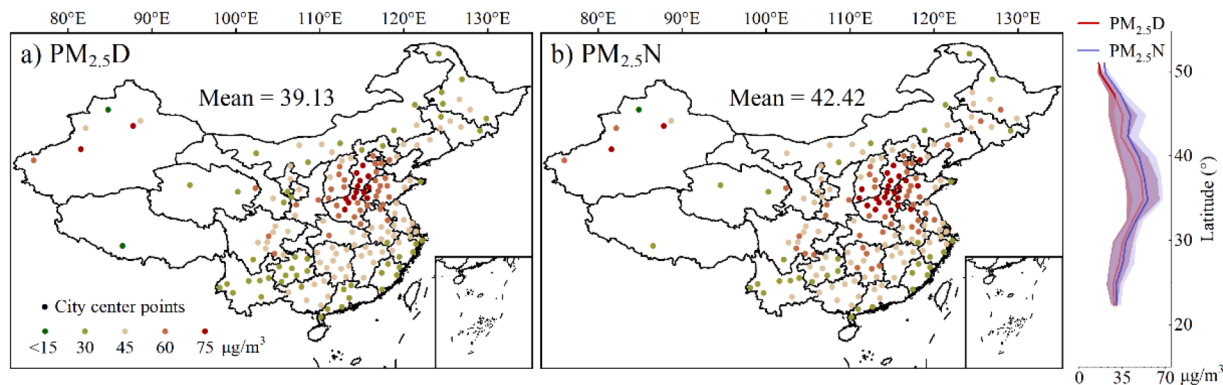


**Fig. 3.** Annual distribution of PM<sub>2.5</sub> over mainland China. (The values located at the city center points represent the averages of all available monitoring stations in that city. The line chart shows the PM<sub>2.5</sub> latitudinal profile, with the shaded area representing  $\pm 1$  S.D.).

also experiences high PM<sub>2.5</sub> levels due to the abundance of desert dust particles (Rupakheti et al., 2021), with two cities exceeding 60 µg/m<sup>3</sup>. Importantly, due to data limitations in some cities, there are gaps in urban statistics in the northeastern and western parts of China.

The highest PM<sub>2.5</sub> levels across all four seasons are found at 33°–40°N latitude (Fig. S2). In spring and autumn, the distribution patterns are similar to the annual average, with peak values concentrated in the central part of North China. In summer, the pollution levels are consistently the lowest, with the smallest difference between daytime and nighttime PM<sub>2.5</sub> levels (0.2 µg/m<sup>3</sup>). During summer, the peak values in the latitudinal profile are only 34.7 (daytime) and 34.5 µg/m<sup>3</sup> (nighttime). This is attributed to frequent rainfall, which causes particle deposition and dilution (Li et al., 2023). In contrast, the pollution levels are highest in winter, with high PM<sub>2.5</sub> concentrations concentrated in North China. Additionally, the areas with high values cover a wider range than those in spring and autumn. During the daytime, 23 % of the cities have PM<sub>2.5</sub> levels exceeding 75 µg/m<sup>3</sup>, whereas at night, this figure increases to 32 %. This is closely related to emissions from coal-fired heating and atmospheric conditions that are unfavorable for pollution dispersion (Ping et al., 2023). In addition to anthropogenic

emissions, high pollution levels in the northwestern region are also significantly caused by dust storms due to the dry environment (Rupakheti et al., 2021).

### 3.1.2. Annual and seasonal distributions of the CUHI/SUHI

The CUHI and SUHI consistently have higher intensities at night than during the day (Fig. 4). CUHI<sub>D</sub>, CUHI<sub>N</sub>, and SUHI<sub>N</sub> all exhibit dual peak values near 45°N and 38°N, with relatively consistent distribution patterns. This indicates a strong UHI distribution in the central and northern parts of North China. Overall, CUHI<sub>D</sub> is positive in 68 % of the cities, whereas CUHI<sub>N</sub> and SUHI<sub>D</sub> are positive in 78 % and 87 % of the cities, respectively. Furthermore, in 98 % of the cities, the SUHI<sub>N</sub> is greater than 0. This difference may arise from the different observation methods used. The CUHI is based on daily maximum/minimum temperatures, which may differ from those of urban and rural stations because of differences in data generation times. The SUHI uses instantaneous data at 1:30 am and 13:30 pm (Wan et al., 2021), with imaging times that are the same for urban and rural areas. Additionally, the SUHI calculations exclude cloudy, rainy, and snowy weather, which could also contribute to the differences compared with the 'all-sky' conditions of

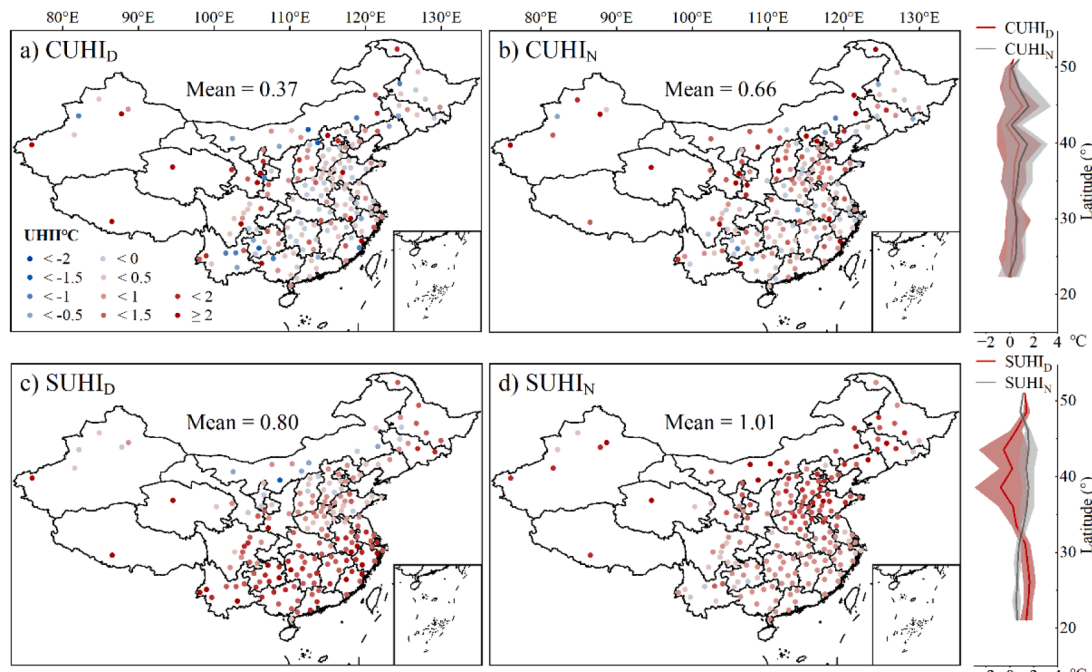


**Fig. 4.** Annual average canopy/surface UHII in mainland China. (The values located at the city center points represent the averages of all available stations/pixels in the city. The line chart shows the CUHI/SUHI latitudinal profile, with the shaded area representing  $\pm 1$  S.D.).

the CUHI.

The CUHI consistently exhibits greater intensities at night than during the day across all four seasons (Fig. S3). The overall distribution trends for the daytime and nighttime UHII are similar, with dual peak values occurring at approximately 40°N and 45°N. During the day, the CUHI is the highest in summer (0.49 °C), which is likely due to the more pronounced heat absorption and warming of impervious materials than those of bare ground and vegetation (Siddiqui et al., 2021). In contrast, the lowest CUHI<sub>D</sub> occurs in winter (UHII = 0.24 °C), with 36 % of the areas exhibiting a cold island effect (UHII < 0 °C). At night, there are no significant differences in the mean CUHI values across the four seasons, with high UHII concentrated in Central China and central-northern North China. In contrast, the SUHI significantly differs between the daytime and nighttime distributions (Fig. S4). At night, the overall trend of the SUHI is similar to that of the CUHI, with high values clustered in central-northern North China across all seasons. During the day, however, the SUHI exhibits distinct distribution patterns compared with those of the CUHI, with high values frequently occurring between 22°N and 28°N and low values concentrated between 38°N and 45°N. Notably, the two significantly low values are attributed to the desert regions in Xinjiang and Inner Mongolia, causing a cold island effect. CUHI<sub>D</sub> does not exhibit this phenomenon because meteorological stations are sparse in desert areas, whereas satellite-derived surface temperature data include these regions.

### 3.2. Differences in UHI across various PM<sub>2.5</sub> levels

To explore the relationships between different pollution levels and the UHII, cities were categorized into high- and low-pollution groups on the basis of the median PM<sub>2.5</sub> levels across all cities. The UHII was subsequently analyzed within these groups (Fig. 5). The daytime and nighttime CUHI in high-PM<sub>2.5</sub> cities are lower than those in low-PM<sub>2.5</sub> cities by -0.11 and -0.14 °C, respectively (Fig. 5b box plot). However, these differences are not statistically significant ( $p > 0.1$ ). In contrast, the SUHI significantly differs between the two pollution levels ( $p < 0.1$ ),

with distinct patterns observed between day and night. Both CUHI<sub>N</sub> and SUHI<sub>N</sub> exhibit a high-high distribution pattern in North China, whereas a low-low relationship is mainly observed in the southeastern coastal areas and the western part of South China. However, it is worth noting that there are a significant number of high-low cities in the central part of North China for the SUHI, which is noticeably greater than that for the CUHI<sub>D</sub>. Compared with other combinations, the relationship between PM<sub>2.5</sub> and SUHI<sub>D</sub> more often exhibits an inverse correlation (67.8 %). In contrast, SUHI<sub>N</sub> has the most extensive high-high distribution, which is also reflected in the comparison of mean values (Fig. 5d), indicating that higher pollution areas correspond to higher nighttime SUHI.

The  $\Delta$ UHII was calculated on the basis of the 25th (Q25) and 75th (Q75) percentiles of the PM<sub>2.5mean</sub> (Fig. 6a). Under clear-sky conditions, both types of UHII are generally lower in high-pollution scenarios than in low-PM<sub>2.5mean</sub> scenarios (except in summer). Among them, the difference in the SUHI<sub>D</sub> is the largest, with a monthly average of -0.23 °C, followed by the CUHI<sub>D</sub> (-0.11 °C), SUHI<sub>N</sub> (-0.10 °C), and CUHI<sub>N</sub> (-0.07 °C). This suggests that high pollution tends to weaken UHII, with a more pronounced effect during the day and on the surface, while having a weaker impact at night and on the canopy. Compared with the CUHI<sub>D</sub>, a larger proportion of cities have a negative  $\Delta$ UHII for the SUHI<sub>D</sub> (Fig. S7-S8). Except for the months from May to September, more than 70 % of the cities present lower SUHI<sub>D</sub> values on high-pollution days, with approximately 25 % of these cities passing the significance test ( $p < 0.1$ ). For both the SUHI<sub>D</sub> and CUHI<sub>D</sub>, the largest negative  $\Delta$ UHII occurs in winter, and this difference has been proven to be significant nationwide. Cities with a positive  $\Delta$ UHII are distributed mainly in southern and southwestern China. In comparison, the trend of heat island reduction caused by PM<sub>2.5mean</sub> levels at night is weaker. Although winter and some spring months present relatively large heat island differences, overall, only approximately half of the months present coverage rates of negative  $\Delta$ UHII values exceeding 50 % (Figs. S9-S10). In spring and autumn, low  $\Delta$ UHII values are mostly concentrated in the North China Plain, whereas high values are primarily distributed in southern and southwestern regions. During summer nights, the highest distribution of

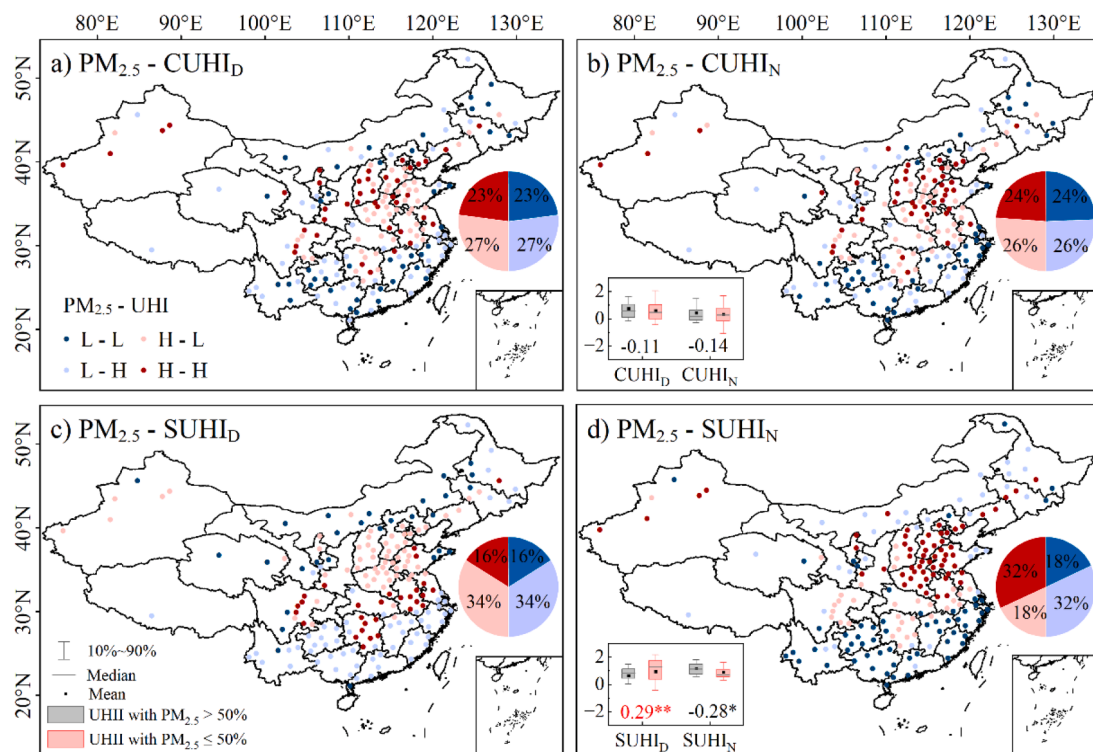


**Fig. 5.** Relationships between different PM<sub>2.5mean</sub> levels and the urban heat island intensity (UHII) based on median division. (The box plot compares the mean UHII based on different PM<sub>2.5</sub> levels. \* and \*\* indicate  $p < 0.1$  and  $p < 0.05$ , respectively.).

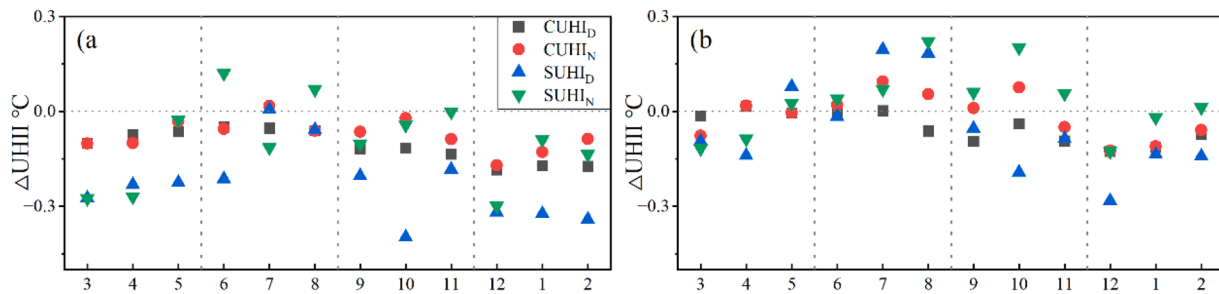


**Fig. 6.** The difference in the UHII between the  $\text{PM}_{2.5\text{mean}} \leq 75\text{th}$  percentile and the  $\text{PM}_{2.5\text{mean}} \geq 25\text{th}$  percentile under (a) clear-sky and (b) all-sky conditions (the symbols in the figure represent the averages across all cities, with details provided in Figs. S5–S6).

positive  $\Delta\text{UHII}$  values is detected, with some months exceeding 65 %. This indicates that high pollution tends to increase the UHII during summer nights.

Compared with clear-sky conditions, the  $\Delta\text{UHII}$  under all-sky conditions shows a smaller negative trend (Fig. 6b). However, in winter, cities still exhibit lower UHII under high-pollution conditions (Figs. S11–S14). At the same time, the warming effect during summer nights is more pronounced, with some autumn months also showing more than 60 % coverage of positive  $\Delta\text{UHII}$  (Fig. S14). Notably, under all-sky conditions, the number of factors influencing the UHII increases, suggesting that the positive  $\Delta\text{UHII}$  anomalies in summer and autumn (Figs. S5–S6) may be due not only to the  $\text{PM}_{2.5\text{mean}}$  but also to other phenomena associated with high-pollution days.

### 3.3. Variations in UHII performance across different levels of daytime/nighttime $\text{PM}_{2.5}$

Under clear-sky conditions, the UHII is lower when  $\text{PM}_{2.5\text{D}} \geq Q_{75\text{th}}$  than when it is lower during daytime pollution conditions (Fig. 7a). The greatest difference is observed in the  $\text{SUHI}_\text{D}$ , with a monthly average of  $-0.21^\circ\text{C}$ , followed by the  $\text{CUHI}_\text{D}$  ( $-0.10^\circ\text{C}$ ),  $\text{SUHI}_\text{N}$  ( $-0.09^\circ\text{C}$ ), and  $\text{CUHI}_\text{N}$  ( $-0.07^\circ\text{C}$ ). This is similar to the  $\Delta\text{UHII}$  categorized by the  $\text{PM}_{2.5\text{mean}}$ , but the differences are slightly smaller in magnitude, indicating that the mechanisms behind the impact on the UHI effect are similar under the two pollution classification methods. The greatest negative  $\Delta\text{UHII}$  appears in winter, followed by autumn, with this phenomenon observed in both the  $\text{SUHI}_\text{D}$  and  $\text{CUHI}_\text{D}$  (Table S2). Although spring exhibits similar trends, both the magnitude and coverage of the negative  $\Delta\text{UHII}$  are significantly lower than those in the aforementioned seasons (Figs. S17–S18). The nighttime UHII also exhibits negative anomalies in many months, especially in spring and winter. Under clear-sky conditions, only the  $\text{SUHI}_\text{N}$  in summer shows the opposite trend, with more than 65 % of the cities exhibiting positive anomalies. In contrast, under all-sky conditions, the number of months with negative anomalies on high-pollution days significantly decreases, and multiple positive signals are observed in summer and autumn.

The  $\Delta\text{UHII}$  categorized by  $\text{PM}_{2.5\text{N}}$  is shown in Fig. 8. Under clear-

sky conditions, the  $\text{SUHI}_\text{N}$  and  $\text{CUHI}_\text{N}$  exhibit differences of only  $-0.08^\circ\text{C}$  and  $-0.06^\circ\text{C}$ , respectively, across different pollution levels, which is even lower than the variations in nighttime UHI caused by  $\text{PM}_{2.5\text{D}}$ . Apart from a notably large negative  $\Delta\text{UHII}$  in winter, no significant positive difference is detected under high  $\text{PM}_{2.5}$  levels during summer nights. Under all-sky conditions, high nighttime pollution significantly increases the nighttime UHII in summer and autumn ( $p < 0.1$ ), with more than 55 % of areas showing a positive  $\Delta\text{UHII}$ . In certain months, this percentage exceeds 65 % ( $\text{CUHI}_\text{N}$  in June–August and  $\text{SUHI}_\text{N}$  in August and October), as shown in Figs. S29–S30.

In summary,  $\text{PM}_{2.5}$  has a significant weakening effect on the daytime UHII, which is most pronounced in winter. For nighttime UHI, high pollution has only a strong weakening effect in winter, whereas in summer, the effect is the opposite. High daytime  $\text{PM}_{2.5}$  concentrations not only negatively impact daytime UHI but also seem to have lasting effects at night, interfering with the study of the effects of  $\text{PM}_{2.5\text{N}}$ . Under all-sky conditions, high nighttime pollution tends to enhance the UHII rather than weaken it, and this phenomenon is commonly observed in summer and autumn.

### 3.4. Correlations between $\text{PM}_{2.5\text{N}}$ and the UHII under restricted daytime conditions

The aforementioned results present an unavoidable issue:  $\text{PM}_{2.5\text{D}}$  also affects the nighttime UHII. To clearly understand the impact of nighttime pollution on UHI, it is necessary to mitigate or eliminate this interference. First, three criteria were established: the median  $\text{PM}_{2.5\text{D}}$ ,  $\text{CUHI}_\text{D}$ , and  $\text{SUHI}_\text{D}$  values (Fig. 9). On the basis of these median values, the strength of the daytime  $\text{PM}_{2.5}/\text{UHII}$  ratio was determined. Nighttime pollution levels were subsequently classified into high- and low-pollution days on the basis of the  $Q_{75}$  and  $Q_{25}$  values of  $\text{PM}_{2.5}$ . The samples classified on the basis of  $\text{CUHI}_\text{D}$  and  $\text{SUHI}_\text{D}$  have an even distribution regardless of whether the nighttime conditions are median- or percentile-based. However, when the median  $\text{PM}_{2.5\text{D}}$  is used as the criterion (Fig. 9a), the samples tend to follow a high-high/low-low day-night correspondence pattern, indicating that higher daytime pollution levels often correspond to higher  $\text{PM}_{2.5\text{N}}$  concentrations at

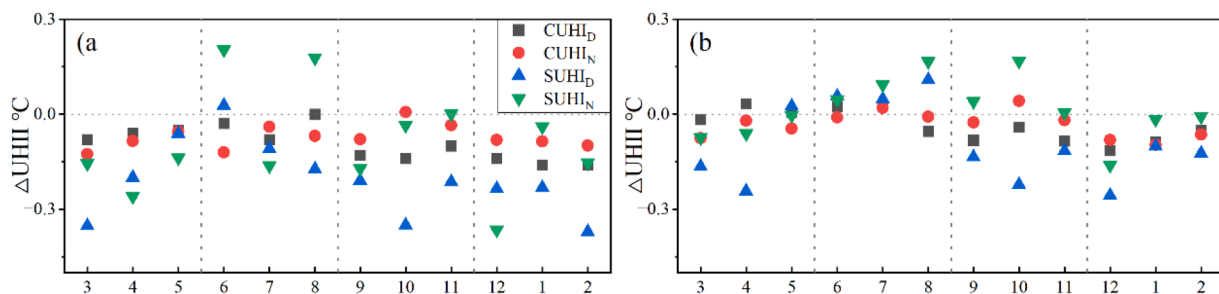


**Fig. 7.** The difference in the UHII between the  $\text{PM}_{2.5\text{D}} \leq 75\text{th}$  percentile and the  $\text{PM}_{2.5\text{D}} \geq 25\text{th}$  percentile under (a) clear-sky and (b) all-sky conditions (symbols in the figure represent the averages across all cities, with details provided in Figs. S15–S16).

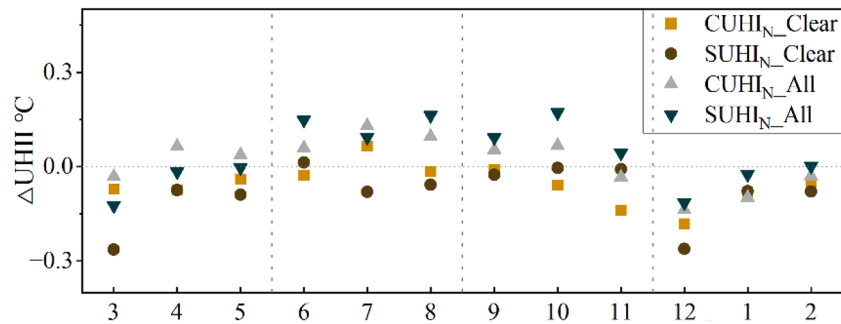


**Fig. 8.** The difference in the UHII between the  $\text{PM}_{2.5}\text{N} \leq 75\text{th}$  percentile and the  $\text{PM}_{2.5}\text{N} \geq 25\text{th}$  percentile under clear-sky and all-sky conditions (the symbols in the figure represent the averages across all cities, with details provided in Figs. S25-S26).

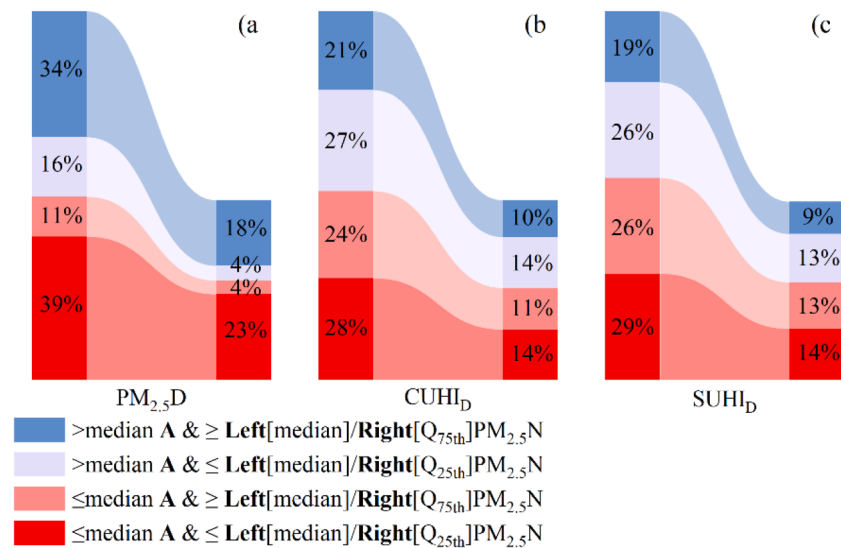


**Fig. 9.** Proportion of  $\text{PM}_{2.5}\text{N}$  samples based on different classification criteria under clear-sky conditions (A represents the elements indicated under the three images).

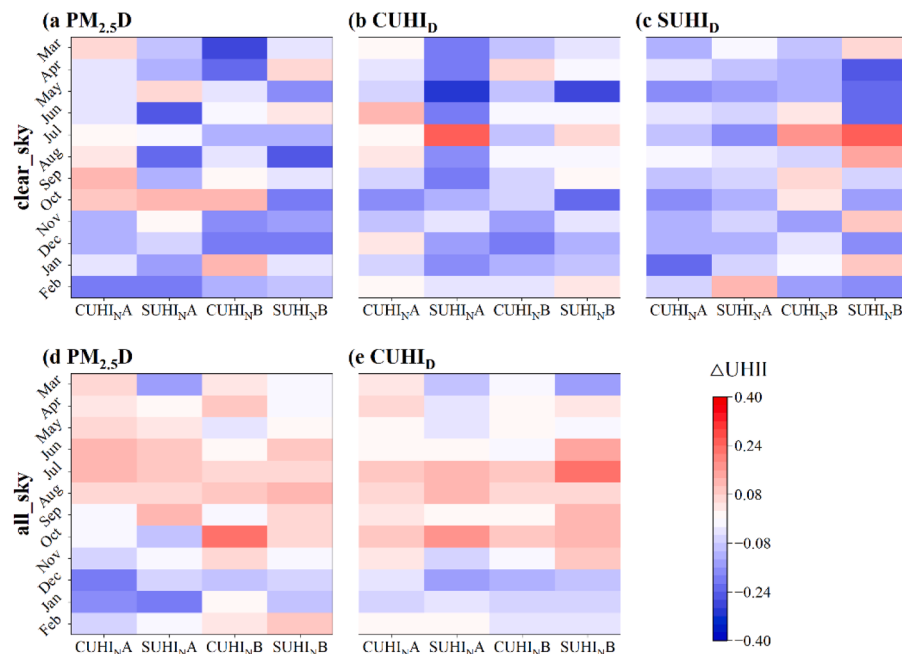


**Fig. 10.** The impact of nighttime pollution on the UHII under different sky conditions, based on A ( $\geq$  median of the top-left element) and B ( $\leq$  median of the top-left element) criteria (the  $\Delta\text{UHII}$  is the difference in the UHII between the  $\text{PM}_{2.5}\text{N} \geq 75\text{th}$  percentile and the  $\text{PM}_{2.5}\text{N} \leq 25\text{th}$  percentile).

night. This pattern is also observed under all-sky conditions (Fig. S31). Since SUHI<sub>D</sub> data predominantly consist of clear-sky conditions, they were not used to ensure the precision of sample partitioning.

The impact of PM<sub>2.5N</sub> on the UHII, which is based on the aforementioned three criteria, is shown in Fig. 10 (details are provided in Supplementary File Text S5). For clear-sky days, after the daytime conditions are constrained, the UHII still exhibits a pattern in most months, where it is lower under high-PM<sub>2.5N</sub> conditions than under low-pollution conditions. By comparison, after the interference of the daytime pollution/heat island intensity is eliminated, the effect of PM<sub>2.5N</sub> on reducing the UHII is somewhat weakened (Table S3). However, notably, under all-sky conditions, after the cooling effect of daytime pollution is mitigated, there is a more pronounced relationship between high PM<sub>2.5N</sub> concentrations and high nighttime UHII (Fig. 10d-e). This indirectly supports our hypothesis that nighttime pollution under all-sky conditions is not the primary cause of the increased heat island intensity. Instead, some factors associated with PM<sub>2.5N</sub> on nonclear-sky days enhance the UHII.

## 4. Discussion

### 4.1. Investigation of the mechanisms of the impact of pollution on the UHI

#### 4.1.1. Mechanism of the impact of PM<sub>2.5</sub> on the UHII under clear-sky conditions

The factors influencing UHI are complex, especially during the daytime (Geng et al., 2023). Therefore, examining only the relationship

between PM<sub>2.5</sub> and the UHII is insufficient for addressing research needs. RF regression models were used to analyze the feature importance of potential influential factors for the UHII in different months for each city (details provided in supplementary file Text S6). The three most important factors for each city were selected and aggregated into an overall dataset. On this basis, the frequency of each factor's occurrence is investigated to determine which factors have the greatest impact on the UHII of cities in mainland China. The results are presented in Fig. 11. For the SUHI<sub>D</sub>, the effect of solar radiation (SR) is the most significant, with the highest values (69 %) occurring in summer. The relative humidity (RH) and percentage of sunshine duration (SD %) rank second and third, respectively, with their peaks also occurring in July. These factors exhibit lower states in winter, where wind speed (WS) becomes the dominant factor, and albedo (Alb) also shows a higher ranking. The impact of PM<sub>2.5</sub> on the SUHI<sub>D</sub> is greater in winter and lower in summer, corresponding with the trend of the seasonal variation in the  $\Delta$ UHII shown in Figs. 6 and 7. The differences in factors influencing the CUHI<sub>D</sub> across different months are similar to those for the SUHI<sub>D</sub>. However, the WS holds a more prominent position among all potential influential factors, with an average frequency exceeding 58 %, whereas Alb ranks the lowest. This discrepancy may be related to the differences in measurement methods between the two datasets.

To better analyze the impact of air pollution on urban heat islands, the average correlations between the three types of PM<sub>2.5</sub> and other potential influential factors in various cities were calculated and are shown in Fig. 12. The degree of pollution and the top-ranked features in terms of importance exhibit significant differences across each month.

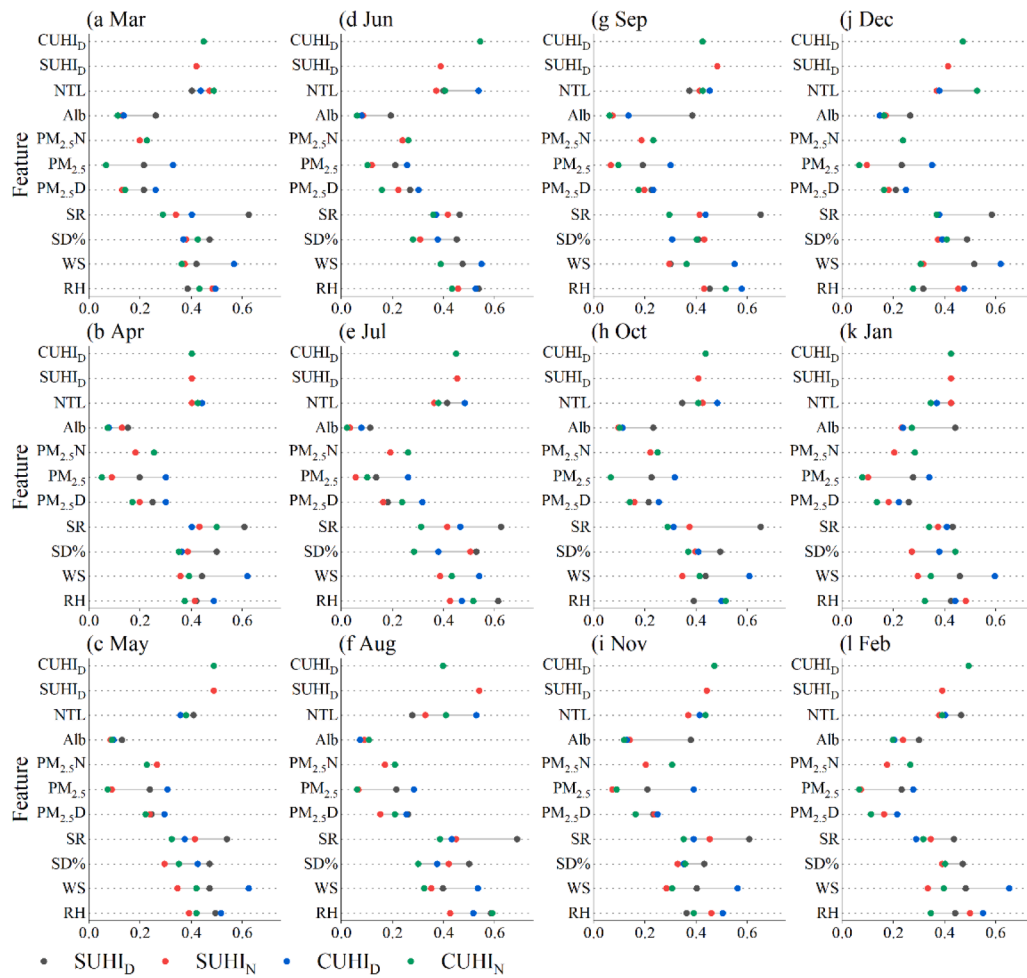


**Fig. 11.** Statistics and frequency of the top three factors in the feature importance ranking under clear-sky conditions for each city (feature importance is derived from the RF regression model, with details presented in Supplementary File Text S6).

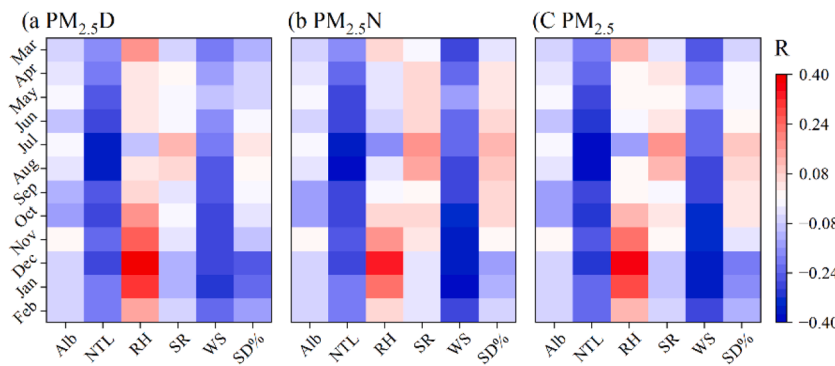


**Fig. 12.** Average correlations between three types of PM<sub>2.5</sub> and other potential influential factors under clear-sky conditions in various cities.

PM<sub>2.5</sub> has a more significant negative correlation with the WS, SD %, and SR in winter than in summer. Notably, these factors, especially the WS, have been confirmed to have a dominant impact on the winter UHII. (Fig. 11j-l). WS reduces heat differences by accelerating heat exchange between urban and rural areas, thereby lowering the urban heat island effect and resulting in a negative correlation with UHI (Chapman et al., 2017; Zhou et al., 2014). Additionally, high WS and high-pollution days rarely coincide because WS accelerates the dispersion of pollutants (Jin et al., 2022; Ping et al., 2023). Particularly in winter, days with low pollution, characterized by low PM<sub>2.5</sub> levels, often correspond to a higher WS, which may explain why the  $\Delta$ UHII has negative values. SR and SD % can directly affect surface heat intake and are positively related to the UHII (Yang et al., 2021; Yang et al., 2020). On days with elevated PM<sub>2.5</sub> levels, an increased number of suspended particulates directly diminishes the incoming shortwave solar radiation, thereby reducing surface heat absorption. The negative correlations between PM<sub>2.5</sub> and SR and SD % are most pronounced in winter, indicating that PM<sub>2.5</sub> has a more significant mitigating effect on the UHII via these pathways. This also accounts for the larger negative  $\Delta$ UHII values observed in this season. RH can increase the hygroscopicity of particles, significantly enhancing their extinction effect (Ting et al., 2022). This characteristic causes the combined influence of RH and PM<sub>2.5</sub> to reduce daytime surface heat, thereby lowering the UHII. However, as the primary factor, the RH exerts a more pronounced influence on the summer UHII, yet its association with PM<sub>2.5</sub> is less evident from June to October. The effect of temporal dislocation leads to a relatively small response of the UHI effect to PM<sub>2.5</sub> during the summer daytime, whereas the UHI effect is more strongly influenced by other natural factors.

The daytime UHII, which serves as the precursor temperature condition for nighttime urban heat islands, is highly important across all months. More than 45 % of the cities identified it as one of the most critical factors influencing the CUHI<sub>D</sub>, whereas 44 % considered it crucial for the SUHI<sub>D</sub>. This also causes the impact of PM<sub>2.5</sub>N on the nighttime UHII to be confounded by the residual effects of PM<sub>2.5</sub>D on daytime heat islands. Polluted aerosols are believed to primarily exhibit a cooling effect in China (Chen et al., 2024), with the reduction of incoming shortwave radiation being four times greater than the increase in longwave radiation (Chakraborty et al., 2021), which corroborates the findings of this study. Previous studies have generally suggested that the RH reduces the emission of surface longwave radiation at night, thereby increasing the nighttime UHII (Sussman et al., 2021; Wang et al., 2016). However, in this study, under clear-sky conditions, this warming effect was not evident, despite stringent control of the precursor conditions (Fig. 10). The nighttime light index (NTL), which is used to characterize the intensity of human activities, is believed to enhance nighttime UHI (Du et al., 2016; Li and Zhou, 2019). However, in this study, the scattering effect of PM<sub>2.5</sub>N on light was predominant, meaning that high pollution levels reduced the radiation detected by sensors (Chen et al., 2023). This phenomenon is clearly reflected in the correlation heatmap (Fig. 12b). Unfortunately, this strong negative

correlation does not provide meaningful insight into the impact of pollution on heat islands in this study. It remains unclear whether this relationship is due to changes in human activities or radiative attenuation caused by particulates. The impact of PM<sub>2.5</sub>N on the nighttime UHII ranks among the top potential influential factors in only 20 % (SUHI<sub>N</sub>) to 25 % (CUHI<sub>N</sub>) of cities, whereas the impact of PM<sub>2.5</sub>mean ranks even lower, at just 7.7 % to 20 %. This value is significantly lower than its impact on the daytime UHII, the values of which range from 22 % to 31 %.

In summary, the impact of nighttime pollution on the UHI<sub>N</sub> is more likely a continuation of the weakening effect of PM<sub>2.5</sub>D on the daytime UHII. The changes in nighttime heat islands are less influenced by pollution than the changes in daytime heat islands are.

#### 4.1.2. The mechanism of the impact of PM<sub>2.5</sub> on the UHII under all-sky conditions

Under all-sky conditions, the factors influencing UHI are more complex. However, 22 % (SUHI<sub>D</sub>) to 26 % (CUHI<sub>D</sub>) of cities still experience a strong impact of PM<sub>2.5</sub>D on the daytime UHII (Fig. S32). Similar to clear-sky days, under all-sky conditions, the SR, RHU, and WS remain among the top potential influential factors. However, the monthly fluctuations in these factors are significantly smaller. The frequency of PM<sub>2.5</sub>D peaks at more than 30 % in winter, making it one of the important factors influencing daytime urban heat islands and associated with the severe pollution emitted by coal-fired heating during winter (Yang et al., 2020). Precipitation (P) and daytime precipitation (PD) are highly important for the UHII in ~10 % of cities, with the highest importance in summer (14 %~25 %) and the lowest importance in winter. This phenomenon is closely related to China's extensive monsoonal climate, where abundant summer precipitation reduces temperatures and narrows the urban-rural temperature difference (Deng et al., 2024; Du et al., 2016). Precipitation promotes particle deposition, resulting in a negative correlation with PM<sub>2.5</sub> (Fig. S33), but this relationship is not particularly evident during summer. Importantly, in this study, P is a quantitative measure, but the amount of precipitation does not always correspond to its duration. Therefore, the cooling effect of precipitation may be underestimated, and its actual impact on the UHI effect could be more significant than the results indicate.

During the nighttime, 42 % (CUHI<sub>N</sub>) and 38 % (SUHI<sub>N</sub>) of the cities regard the daytime UHII as the primary influential factor. This finding indicates that the nighttime UHI on all-sky days is also influenced by this continuity of thermal conditions. While the ranking of the importance of other factors shows minimal differences compared with clear-sky conditions, precipitation explains nighttime heat island variations in 10–15 % of cities. Additionally, the correlation between PM<sub>2.5</sub>N and precipitation ranges from -0.16 (PN) to -0.19 (P), which is significantly greater than that between PM<sub>2.5</sub>D and precipitation. The correlation results with SR and SD % also indicate that high PM<sub>2.5</sub>N from April to October corresponds to high surface thermal environments, which is particularly evident in summer. We hypothesize that this is due to the frequent

occurrence of cloudy and rainy days in summer, which correspond to lower nighttime PM<sub>2.5</sub> levels. To validate this hypothesis, clear-sky days were isolated from all-sky conditions, retaining only days with SD percentages less than 60 % (Fig. S34). Under nonclear-sky conditions, low PM<sub>2.5</sub> tends to correlate with lower incoming surface radiation. Overcast days are associated with high incoming radiation and high PM<sub>2.5</sub>, whereas rainy days are associated with lower incoming radiation and low PM<sub>2.5</sub>. This positive correlation may partially explain the positive  $\Delta\text{UHII}$  observed during high-pollution conditions in some months. In essence, under all-sky conditions, PM<sub>2.5N</sub> in summer does not directly affect the UHII. Instead, it corresponds to different incoming surface heat associated with clear (overcast)/rainy conditions classified by high/low nighttime pollution days.

In Fig. 8, the impact of daytime conditions on the relationship between PM<sub>2.5N</sub> and UHI is examined. Under clear-sky conditions, the PM<sub>2.5N</sub> concentration tends to negatively correlate with the nighttime UHII. However, under all-sky conditions, a positive  $\Delta\text{UHII}$  is more frequently observed. PM<sub>2.5N</sub> has been widely confirmed to have an insulating effect on the surface at night by generating aerosols that absorb longwave radiation (Cao et al., 2016; Yang et al., 2020). Under clear sky conditions, this effect is diminished because of the lack of optimal aerosol condensation conditions, and PM<sub>2.5</sub> is more likely to be reduced by the turbulent diffusion of heat conduction (Li et al., 2018), explaining the negative correlation. Under all-sky conditions, without the influence of daytime UHII continuity, the insulating effect of PM<sub>2.5</sub> is more prominent.

#### 4.2. Differences and uncertainties in the results

Previous studies have shown that PM<sub>2.5</sub> weakens daytime UHI (Li et al., 2018; Yang et al., 2020), which is consistent with the findings of this research. However, there are some differences between the results of this study and previous results regarding the weakening/enhancing effects of nighttime pollution on UHI. These discrepancies may be due to differences in the chosen study periods. To minimize differences in the temperature conditions caused by variations in radiation, this study restricted the total samples to the same month. When this restriction is relaxed to an entire season, such as in the case of clear-sky days in winter in Beijing, the number of days with PM<sub>2.5</sub> levels exceeding 75 and 90  $\mu\text{g}/\text{m}^3$  in February 2015~2023 is 31 and 22, respectively, whereas in December 2015~2023, the numbers are 11 and 8, respectively. This leads to an overrepresentation of February data and an underrepresentation of December data during the statistical analysis. The maximum difference in sunshine duration between these months can reach 2 h, resulting in significant variations in surface radiation exposure. Furthermore, this study revealed that when correlations are explored, the use of different cities within the same month can be misleading. This is more likely due to differences in background climate rather than specific relationships between particular factors (Zhao et al., 2014).

Despite thoroughly discussing the relationships between pollution and the UHII and their impact mechanisms, this study did not include differences across various climate zones due to space limitations. The UHII is an element with significant spatial heterogeneity (Peng et al., 2018; Ziter et al., 2019). Future research should focus more on discussing differences across dry, wet, and climate variations. The LST data used to characterize the SUHI in this study can be affected by cloud cover, potentially leading to overestimations of pixel temperatures in certain urban/rural areas when the results are analyzed under all-sky conditions. Although we used data from multiple cities to balance this error as much as possible and found consistency with CUHI changes, excluding cloud interference to obtain more precise LST data would enhance the accuracy of the results. Additionally, the results of this study predominantly highlight the radiative forcing effect of PM<sub>2.5</sub> during the daytime. However, the aerosol dynamic effects of PM<sub>2.5</sub>, which alter the planetary boundary layer and convective intensity to influence the UHII (Han et al., 2020), were not included in this research.

This represents a potential avenue for future exploration.

## 5. Conclusion

This study, which uses refined pollution intensity classification and comparative methods, delves into the relationships between pollution and the UHI effect in mainland China, as well as the underlying mechanisms. Research has revealed that cities with high PM<sub>2.5</sub> levels often exhibit high nighttime UHI. Under clear-sky conditions, both the PM<sub>2.5mean</sub> and the PM<sub>2.5D</sub> reduce the daytime and nighttime UHII, and the PM<sub>2.5N</sub> similarly reduces the nighttime UHII. The magnitude of this cooling effect peaks in winter and is minimal in summer. However, under all-sky conditions, the heat-reducing effect of PM<sub>2.5</sub> is suppressed, and in some months, it even enhances the UHII. Daytime pollution has been demonstrated to primarily diminish UHI by scattering or reflecting radiation from particulate matter. Under high humidity conditions, PM<sub>2.5</sub> combines with atmospheric moisture to form aerosols that further reduce the daytime UHII through increased radiative forcing. Wind speed facilitates heat exchange between urban and rural areas and promotes the dispersion of pollution, leading to low wind speed days being correlated with high-pollution days. This mechanism is particularly evident in winter, when the effect of pollution on reducing UHI is more pronounced. The heat conditions during the day set the stage for the nighttime UHII, driving nighttime heat island changes. Under all-sky conditions, the impact of PM<sub>2.5N</sub> on the UHII in summer is not direct but is instead due to the differences in incoming surface heat between clear (overcast) and rainy conditions associated with high/low nighttime pollution days.

This study also indicates that when various pollution conditions and their associations with the UHII over an extended period are compared, discrepancies in the sample size on days of high pollution and the related variations in incoming radiation across different months might obscure the true findings. The correlation between PM<sub>2.5</sub> and UHI across cities can also be blurred by background climate variations. Therefore, similar background and radiation conditions are essential for accurate research. Our study enhances the understanding of the impact of particulate matter on UHI and establishes strict guidelines for studying thermal and pollution environments, providing scientific guidance for future urban management.

## CRediT authorship contribution statement

**Zihao Feng:** Writing – original draft, Data curation. **Xuhong Wang:** Writing – review & editing, Conceptualization. **Mengqianxi Yu:** Visualization, Investigation. **Yimei Yuan:** Resources. **Bingqian Li:** Methodology.

## Declaration of competing interest

The authors declare that they have no known competing financial interests or personal relationships that could have appeared to influence the work reported in this paper.

## Acknowledgment

The authors are indebted to China Meteorological Data Service Center for archiving Meteorological datasets, China National Environmental Monitoring Centre for PM<sub>2.5</sub> datasets, Copernicus Climate Change Service for reanalysis data, NASA for archiving MODIS datasets, U.S. Geological Survey for archiving digital elevation model and the National Centers for Environmental Information for sky condition total coverage datasets. The authors acknowledge the financial support provided by The National Natural Science Foundation of China (41971387).

## Supplementary materials

Supplementary material associated with this article can be found, in the online version, at [doi:10.1016/j.scs.2024.106001](https://doi.org/10.1016/j.scs.2024.106001).

## Data availability

Data will be made available on request.

## References

- Ali, M. A., Elsayed, A., Elkabani, I., Youssef, M. E., & Hassan, G. E. (2024). Modeling global solar radiation using ambient temperature. *Cleaner Energy Systems*, 7, Article 100101.
- Aparicio, A. J. P., Carrasco, V. M. S., Montero-Martín, J., Sanchez-Lorenzo, A., Costa, M. J., & Antón, M. (2023). Analysis of sunshine duration and cloud cover trends in Lisbon for the period 1890–2018. *Atmospheric Research*, 290, Article 106804.
- Breiman, L. (2001). Random forests. *Machine learning*, 45, 5–32.
- Cao, C., Lee, X., Liu, S., Schultz, N., Xiao, W., Zhang, M., & Zhao, L. (2016). Urban heat islands in China enhanced by haze pollution. *Nature communications*, 7(1), 1–7.
- Chakraborty, T., & Lee, X. (2019). A simplified urban-extent algorithm to characterize surface urban heat islands on a global scale and examine vegetation control on their spatiotemporal variability. *International Journal of Applied Earth Observation and Geoinformation*, 74, 269–280.
- Chakraborty, T., Lee, X., & Lawrence, D. M. (2021). Strong Local Evaporative Cooling Over Land Due to Atmospheric Aerosols. *Journal of Advances in Modeling Earth Systems*, 13(5), Article e2021MS002491.
- Chapman, S., Watson, J. E. M., Salazar, A., Thatcher, M., & McAlpine, C. A. (2017). The impact of urbanization and climate change on urban temperatures: a systematic review. *Landscape Ecol*, 32(10), 1921–1935.
- Chen, A., Zhao, C., Zhang, H., Yang, Y., & Li, J. (2024). Surface albedo regulates aerosol direct climate effect. *Nature Communications*, 15(1), 7816.
- Chen, H., Xu, Y., Zhong, S., Mo, Y., & Zhu, S. (2023). Mapping nighttime PM2.5 concentrations in Nanjing, China based on NPP/VIIRS nighttime light data. *Atmos. Environ.*, 303, Article 119767.
- Cui, F., Hamdi, R., Yuan, X., He, H., Yang, T., Kuang, W., Termonia, P., & De Maeyer, P. (2021). Quantifying the response of surface urban heat island to urban greening in global north megacities. *Science Total Environment*, 801, Article 149553.
- Deng, X., Yu, W., Shi, J., Huang, Y., Li, D., He, X., Zhou, W., & Xie, Z. (2024). Characteristics of surface urban heat islands in global cities of different scales: Trends and drivers. *Sustainable Cities and Society*, 107, Article 105483.
- Du, H., Wang, D., Wang, Y., Zhao, X., Qin, F., Jiang, H., & Cai, Y. (2016). Influences of land cover types, meteorological conditions, anthropogenic heat and urban area on surface urban heat island in the Yangtze River Delta Urban Agglomeration. *Science Total Environment*, 571, 461–470.
- Fahed, J., Kinab, E., Ginechet, S., & Adolphe, L. (2020). Impact of urban heat island mitigation measures on microclimate and pedestrian comfort in a dense urban district of Lebanon. *Sustainable Cities and Society*, 61, Article 102375.
- Feng, Z., Wang, X., Yuan, J., Zhang, Y., & Yu, M. (2023). Changes in air pollution, land surface temperature, and urban heat islands during the COVID-19 lockdown in three Chinese urban agglomerations. *Science Total Environment*, 892, Article 164496.
- Friedl, M., & Sulla-Menashe, D. (2022). MODIS/Terra+Aqua land cover type yearly L3 global 500m sin grid V061 [Data set]. NASA EOSDIS Land Processes Distributed Active Archive Center. <https://doi.org/10.5067/MODIS/MCD12Q1.061> Accessed 2023-11-20 from.
- Gabriel, K. M. A., & Endlicher, W. R. (2011). Urban and rural mortality rates during heat waves in Berlin and Brandenburg, Germany. *Environment Pollution*, 159(8), 2044–2050.
- Geng, X., Zhang, D., Li, C., Yuan, Y., Yu, Z., & Wang, X. (2023). Impacts of climatic zones on urban heat island: Spatiotemporal variations, trends, and drivers in China from 2001–2020. *Sustainable Cities and Society*, 89, Article 104303.
- Guo, J., Yin, Y., Xu, M., Wu, J., Liu, D., Fan, W., & Lu, P. (2022). Numerical study of aerosol radiative forcing over East Asia and the impacts of cloud coverage and relative humidity. *Atmospheric Research*, 273, Article 106168.
- Han, W., Li, Z., Wu, F., Zhang, Y., Guo, J., Su, T., Cribb, M., Fan, J., Chen, T., Wei, J., & Lee, S.-S. (2020). The mechanisms and seasonal differences of the impact of aerosols on daytime surface urban heat island effect. *Atmospheric Chemistry and Physics*.
- He, Y., Wu, C., & Fan, Y. (2024). Exploring the drivers of local government budget coordination: A random forest regression analysis. *International Review of Economics & Finance*, 93, 1104–1113.
- Huang, X., Wang, Z., & Ding, A. (2018). Impact of Aerosol-PBL interaction on haze pollution: Multiyear observational evidences in North China. *Geophysical Research Letters*, 45(16), 8596–8603.
- Jacobson, M. Z. (1998). Studying the effects of aerosols on vertical photolysis rate coefficient and temperature profiles over an urban airshed. *Journal of Geophysical Research: Atmospheres*, 103(D9), 10593–10604.
- Jin, H., Zhong, R., Liu, M., Ye, C., & Chen, X. (2022). Spatiotemporal distribution characteristics of PM2.5 concentration in China from 2000 to 2018 and its impact on population. *Journal of Environmental Management*, 323, Article 116273.
- Keys, R. (1981). Cubic convolution interpolation for digital image processing. *IEEE Transactions on Acoustics, Speech, and Signal Processing*, 29(6), 1153–1160.
- Li, H., Meier, F., Lee, X., Chakraborty, T., Liu, J., Schaap, M., & Sodoudi, S. (2018). Interaction between urban heat island and urban pollution island during summer in Berlin. *Science Total Environment*, 636, 818–828.
- Li, J., Zhou, M., Lenschow, D. H., Cheng, Z., & Dou, Y. (2020). Observed relationships between the urban heat island, urban pollution island, and downward longwave radiation in the Beijing area. *Earth and Space Science*, 7(6), Article e2020EA001100.
- Li, S., Chenghu, Z., & Qu, M. (2023). Spatiotemporal variations and mechanism of PM2.5 pollution in urban area: The case of Guiyang, Guizhou, China. *Journal of Environmental Management*, 341, Article 118030.
- Li, X., & Zhou, W. (2019). Spatial patterns and driving factors of surface urban heat island intensity: A comparative study for two agriculture-dominated regions in China and the USA. *Sustainable Cities and Society*, 48, Article 101518.
- Liu, Y., Cao, G., Zhao, N., Mulligan, K., & Ye, X. (2018). Improve ground-level PM2.5 concentration mapping using a random forests-based geostatistical approach. *Environmental Pollution*, 235, 272–282.
- Liu, Z., Lai, J., Zhan, W., Bechtel, B., Voogt, J., Quan, J., Hu, L., Fu, P., Huang, F., & Li, L. (2022). Urban heat islands significantly reduced by COVID-19 lockdown. *Geophysical Research Letters*, 49(2), Article e2021GL096842.
- Manoli, G., Faticchi, S., Schläpfer, M., Yu, K., Crowther, T. W., Meili, N., Burlando, P., Katul, G. G., & Bou-Zeid, E. (2019). Magnitude of urban heat islands largely explained by climate and population. *Nature*, 573(7772), 55–60.
- McMillin, L. M. (1975). Estimation of sea surface temperatures from two infrared window measurements with different absorption. *Journal of Geophysical Research (1896–1977)*, 80(36), 5113–5117.
- Muñoz Sabater, J. (2019). ERA5-Land monthly averaged data from 1950 to present. *Copernicus Climate Change Service (C3S) Climate Data Store (CDS)*. <https://doi.org/10.24381/cds.68d2bb30> (Accessed on 23-12-2023).
- Oke, T. (1973). City Size and the Urban Heat Island. *Atmos. Environ.*, 7, 769–779.
- Oke, T.R., 1984. Methods in urban climatology.
- Peng, J., Ma, J., Liu, Q., Liu, Y., Hu, Y.n., Li, Y., & Yue, Y. (2018). Spatial-temporal change of land surface temperature across 285 cities in China: An urban-rural contrast perspective. *Science of the Total Environment*, 635, 487–497.
- Peng, S., Piao, S., Ciais, P., Friedlingstein, P., Ottle, C., Breon, F.-M., Nan, H., Zhou, L., & Myneni, R. (2011). Surface Urban Heat Island Across 419 Global Big Cities. *Environmental Science & Technology*, 46, 696–703.
- Ping, L., Wang, Y., Lu, Y., Lee, L.-C., & Liang, C. (2023). Tracing the sources of PM2.5-related health burden in China. *Environment Pollution*, 327, Article 121544.
- Román, M. O., Wang, Z., Sun, Q., Kalb, V., Miller, S. D., Molthan, A., Schultz, L., Bell, J., Stokes, E. C., Pandey, B., Seto, K. C., Hall, D., Oda, T., Wolfe, R. E., Lin, G., Golpayegani, N., Devadiga, S., Davidson, C., Sarkar, S., Praderas, C., Schmaltz, J., Boller, R., Stevens, J., Ramos González, O. M., Padilla, E., Alonso, J., Detrés, Y., Armstrong, R., Miranda, I., Conte, Y., Marrero, N., MacManus, K., Esch, T., & Masuoka, E. J. (2018). NASA's Black Marble nighttime lights product suite. *Remote Sensing of Environment*, 210, 113–143.
- Rupakheti, D., Yin, X., Rupakheti, M., Zhang, Q., Li, P., Rai, M., & Kang, S. (2021). Spatio-temporal characteristics of air pollutants over Xinjiang, northwestern China. *Environment Pollution*, 268, Article 115907.
- Ryu, Y.-H., & Baik, J.-J. (2012). Quantitative analysis of factors contributing to urban heat island intensity. *Journal of Applied Meteorology and Climatology*, 51, 842–854.
- Sarrat, C., Lemonsu, A., Masson, V., & Guedalia, D. (2006). Impact of urban heat island on regional atmospheric pollution. *Atmospheric Environment*, 40(10), 1743–1758.
- Siddiqui, A., Kushwaha, G., Nikam, B., Srivastav, S. K., Shelar, A., & Kumar, P. (2021). Analysing the day/night seasonal and annual changes and trends in land surface temperature and surface urban heat island intensity (SUHII) for Indian cities. *Sustainable Cities and Society*, 75, Article 103374.
- Sun, M., Zhao, N., & Zheng, E. Y. (2024). The devil in the air: Air pollution and dementia. *Journal of Environmental Economics and Management*, 127, Article 103020.
- Sussman, H. S., Dai, A., & Roundy, P. E. (2021). The controlling factors of urban heat in Bengaluru, India. *Urban Climate*, 38, Article 100881.
- Ting, Y.-C., Young, L.-H., Lin, T.-H., Tsay, S.-C., Chang, K.-E., & Hsiao, T.-C. (2022). Quantifying the impacts of PM2.5 constituents and relative humidity on visibility impairment in a suburban area of eastern Asia using long-term in-situ measurements. *Science of the Total Environment*, 818, Article 151759.
- Tran, H., Uchihama, D., Ochi, S., & Yasuoka, Y. (2006). Assessment with satellite data of the urban heat island effects in Asian mega cities. *International Journal of Applied Earth Observation and Geoinformation*, 8(1), 34–48.
- Ulpiiani, G. (2021). On the linkage between urban heat island and urban pollution island: Three-decade literature review towards a conceptual framework. *Science of the Total Environment*, 751, Article 141727.
- Wan, Z., Hook, S., & Hulley, G. (2021). MODIS/Aqua land surface temperature/emissivity daily L3 global 1km sin grid V061 [Data set]. NASA EOSDIS Land Processes DAAC. <https://doi.org/10.5067/MODIS/MYD11A1.061> Accessed 2023-12-10 from.
- Wang, J., Huang, B., Fu, D., Atkinson, P. M., & Zhang, X. (2016). Response of urban heat island to future urban expansion over the Beijing-Tianjin-Hebei metropolitan area. *Applied Geography*, 70(70), 26–36.
- Wang, J., Qiu, Y., He, S., Liu, N., Xiao, C., & Liu, L. (2018). Investigating the driving forces of NOx generation from energy consumption in China. *Journal of Cleaner Production*, 184, 836–846.
- Wang, Y., Zhao, P., Xiao, H., & Zhang, P. (2024). Aerosol effects on liquid cloud microphysical properties in south China: Land-ocean contrasts. *Atmospheric Pollution Research*, 15(3), Article 102032.
- Yang, G., Ren, G., Zhang, P., Xue, X., Tysa, S. K., Jia, W., Qin, Y., Zheng, X., & Zhang, S. (2021). PM2.5 Influence on Urban Heat Island (UHI) Effect in Beijing and the Possible Mechanisms. *Journal of Geophysical Research: Atmospheres*, 126(17), Article e2021JD035227.

- Yang, Y., Zheng, Z., Yim, S. H. L., Roth, M., Ren, G., Gao, Z., Wang, T., Li, Q., Shi, C.-e., Ning, G., & Li, Y. (2020). PM2.5 pollution modulates wintertime urban heat island intensity in the beijing-tianjin-hebei megalopolis, China. *Geophysical Research Letters*, 47.
- Yousefi, R., Shaheen, A., Wang, F., Ge, Q., Wu, R., Lelieveld, J., Wang, J., & Su, X. (2023). Fine particulate matter (PM2.5) trends from land surface changes and air pollution policies in China during 1980–2020. *J. Environ. Manage.*, 326, Article 116847.
- Zar, J. H. (2005). Spearman rank correlation. *Encyclopedia of Biostatistics*, 7.
- Zhao, C., Sun, Y., Yang, J., Li, J., Zhou, Y., Yang, Y., Fan, H., & Zhao, X. (2024a). Observational evidence and mechanisms of aerosol effects on precipitation. *Science Bulletin*, 69(10), 1569–1580.
- Zhao, K., Zhu, G., Sang, L., Liu, J., Wang, L., Liu, Y., Xu, Y., Lin, X., Zhang, W., & Ye, L. (2023). Temporal and spatial variation of cloud cover in arid regions of Central Asia in the last 40 years. *Research in Cold and Arid Regions*, 15(2), 66–72.
- Zhao, L., Lee, X., Smith, R. B., & Oleson, K. (2014). Strong contributions of local background climate to urban heat islands. *Nature*, 511(7508), 216–219.
- Zhao, Z., Li, Y., & Su, X. (2024b). Mountains block and seas move: The impact of geographical environment on the China's Carbon Emissions Trading Scheme in reducing urban PM2.5 concentrations. *Sustainable Cities and Society*, 112, Article 105630.
- Zhou, D., Zhao, S., Liu, S., Zhang, L., & Zhu, C. (2014). Surface urban heat island in China's 32 major cities: Spatial patterns and drivers. *Remote Sensing of Environment*, 152, 51–61.
- Zhou, M., He, G., Liu, Y., Yin, P., Li, Y., Kan, H., Fan, M., Xue, A., & Fan, M. (2015). The associations between ambient air pollution and adult respiratory mortality in 32 major Chinese cities, 2006–2010. *Environmental Research*, 137, 278–286.
- Ziter, C. D., Pedersen, E. J., Kucharik, C. J., & Turner, M. G. (2019). Scale-dependent interactions between tree canopy cover and impervious surfaces reduce daytime urban heat during summer. *Proceedings of the National Academy of Sciences*, 116(15), 7575–7580.